Benzenesulfonic acid-grafted UIO-66 with improved hydrophobicity as a stable Brønsted acid catalyst

DOI:
10.1007/s11705-022-2285-5

Document Version
Final published version

Published in:
Frontiers of Chemical Science and Engineering

Front. Chem. Sci. Eng.
https://doi.org/10.1007/s11705-022-2285-5

RESEARCH ARTICLE

Benzenesulfonic acid-grafted UIO-66 with improved hydrophobicity as a stable Brønsted acid catalyst

Zongliang Kou[1], Guanlun Sun[1], Qiuyan Ding[1], Hong Li (✉)[1], Xin Gao[1,2], Xiaolei Fan (✉)[3,4], Xiaoxia Ou[4], Qinhe Pan (✉)[5]

1 School of Chemical Engineering and Technology, National Engineering Research Center of Distillation Technology, Collaborative Innovation Center of Chemical Science and Engineering (Tianjin), Tianjin University, Tianjin 300072, China
2 Haihe Laboratory of Sustainable Chemical Transformations, Tianjin 300192, China
3 Department of Chemical Engineering, School of Engineering, The University of Manchester, Manchester M13 9PL, UK
4 Nottingham Ningbo China Beacons of Excellence Research and Innovation Institute, University of Nottingham Ningbo China, Ningbo 315100, China
5 Key Laboratory of Ministry of Education for Advanced Materials in Tropical Island Resources, School of Chemical Engineering and Technology, Hainan University, Haikou 570228, China

Abstract Hydrothermal and catalytic stability of UIO-66 MOFs with defective structures are critical aspects to be considered in their catalytic applications, especially under the conditions involving water, moisture and/or heat. Here, we report a facile strategy to introduce the macromolecular acid group to UIO-66 to improve the stability of the resulting UIO-66−$PhSO_3H$ MOF in aqueous phase catalysis. In detail, UIO-66−$PhSO_3H$ was obtained by grafting benzenesulfonic acid on the surface of the pristine UIO-66 to introduce the hydrophobicity, as well as the Brønsted acidity, then assessed using catalytic hydrolysis of cyclohexyl acetate (to cyclohexanol) in water. The introduction of hydrophobic molecules to UIO-66 could prevent the material from being attacked by hydroxyl polar molecules effectively, explaining its good structural stability during catalysis. UIO-66−$PhSO_3H$ promoted the conversion of cyclohexyl acetate at ca. 87%, and its activity and textural properties were basically intact after the cyclic stability tests. The facile modification strategy can improve the hydrothermal stability of UIO-66 significantly, which can expand its catalytic applications in aqueous systems.

Keywords metal−organic frameworks (MOFs), UIO-66, hydrolysis of cyclohexyl acetate, hydrophobicity, Brønsted acidity

Received September 29, 2022; accepted November 18, 2022

E-mails: lihongtju@tju.edu.cn (Li H.), xiaolei.fan@manchester.ac.uk (Fan X.), panqh@hainanu.edu.cn (Pan Q.)

1 Introduction

Metal–organic frameworks (MOFs) have received extensive attention in heterogeneous catalysis due to their highly tunable pore structure and chemical composition since their discovery [1,2]. With nearly 20 years of rapid development, MOFs have become one of the most promising materials for catalytic applications [3,4]. However, the stability of MOFs is one of the major concerns for catalytic applications, in which the use of organic and aqueous solvents, elevated temperatures, and/or acidic and basic reagents is common [5]. Hence, the development of structurally stable MOFs for different catalytic reactions is a key research area [5]. Zirconium UIO-66 MOF has shown high thermal and chemical stability due to the high coordination numbers of Zr, as well as its coordination geometry [6]. In addition, during the preparation of UIO-66, different modulators (such as hydrochloric acid or monocarboxylic acid) can be used to alter its framework to create missing linkers and/or defects which can modify its specific surface area and pore volume, as well as introducing Lewis acidity [7]. Compared to Lewis acid catalysts, exploration of Brønsted acid chemistry in MOFs is another interesting topic [8]. Yet it is worth noting that one-pot synthesis methods are difficult to introduce Brønsted acid sites into MOFs because active acidic protons can interfere with the assembly of MOFs during the synthesis [9].

With the further understanding of the physiochemical properties of MOFs in recent years, the concept of ordered intra-heterogeneity [10], post-synthetic modification

(PSM) [11,12], and multivariate [13,14] methods have provided new development opportunities for preparing MOFs with Brønsted acidity. Sulfuric acid with strong acidity was often used to prepare MOFs with super-strong Brønsted acidity. For example, in catalytic biomass conversion, Chen et al. [15] used sulfonic acid-functionalized MOFs as the solid acid catalysts for the selective conversion of fructose to 5-hydroxymethylfurfural with a high conversion of about 90%. However, the PSM method employed by Chen et al. is cumbersome, which required tedious drying procedure to obtain sulfonated UIO-66 with defective structures. Desidery et al. [16] synthesized a fully sulfonated hydrated UIO-66 for catalytic esterification to produce ethyl levulinate, in which the sulfonated UIO-66 enabled the highest yield of ethyl levulinate, while the pristine UIO-66 was least efficient.

However, as the sulfonic acid group is hydrophilic, hence in addition to introducing Brønsted acidity to UIO-66, it also makes UIO-66 hydrophilic, which is not ideal for catalysis in aqueous media. Also, in many catalytic reactions, water was either used as the reactant or produced as the product, hence water is prone to bind with sulfonic acid groups and structural defects in the framework of MOFs, resulting in the deactivation of the catalytic sites [17,18]. A recent study has shown that an increase in surface wettability of the catalyst leads to a decrease in the conversion and selectivity [19]. Therefore, tuning the surface wettability to be hydrophobic can be beneficial to prevent water from attacking MOFs and increase the accessibility of active sites to organic substrates. Among many construction methods to make hydrophobic catalysts, secondary construction, a PSM method, is promising to prepare MOFs-based catalysts with Brønsted acidity [10]. Cai et al. [20] reported a core–shell MOF@COF hybrid NH_2-MIL-101(Fe)@NTU material for styrene oxidation. In details, a series of NH_2-MIL-101(Fe)@NTU-COFs with shell thicknesses ranging from 6 to 40 nm (MIL@NTU*x*, *x* = 1, 2, 3, 4, or 5) were prepared by a two-step method. The findings showed that an increase in the shell thickness (from 20 to 40 nm) increases the water contact angle of the hybrid materials from 118.0° to 137.1°, and the hydrophobic MIL@NTU*x* showed much higher selectivity to the target product benzaldehyde than the pristine NH_2-MIL-101(Fe) MOF (ca. 26.8% after 12 h). Isaka et al. [21] grafted anhydrides (with different chain lengths) onto MIL-125-NH_2 to prepare hydrophobic MOF catalysts for photocatalytic production of H_2O_2 in a two-phase system (of benzyl alcohol/water) under visible light. When the hydrophobic MIL-125-R was used as the catalyst, the H_2O_2 production was four times higher than that achieved by the pristine hydrophilic MIL-125-NH_2 MOF.

In this work, a simple secondary construction PSM method was developed to prepare hydrophobic UIO-66 MOF with good structural stability in catalytic hydrolysis of cyclohexyl acetate to cyclohexanol. By using the secondary construction method, benzenesulfonic acid was successfully grafted to the organic linker of UIO-66 to obtain the hydrophobic Brønsted acid catalyst. The catalytic performance and reusability of the catalysts were assessed, and the findings show that under the optimal conditions the conversion of cyclohexyl acetate can reach ca. 87%, and the catalyst stability is maintained after the cyclic tests.

2 Experimental

2.1 Chemicals

N,*N*-Dimethylformamide (DMF) (≥99.5%), cyclohexyl acetate (≥98%), and acetic acid (>98%) were purchased from Aladdin. Chlorobenzene (≥99.5), absolute ethanol (≥99.8%), and dichloromethane (>99%) were purchased from McLean. 1,4-Benzenedicarboxylic acid (>98%) was purchased from Ron's reagent, $ZrCl_4$ (>98%) was purchased from Merrill, and 4-chlorobenzenesulfonic acid (>98%) was purchased from Bidder. All chemicals were used as received.

2.2 Synthesis of the pristine UIO-66

Figure 1 shows the schematic diagram of catalyst preparation. In detail, UIO-66 was prepared using the method described elsewhere [22,23] via a continuous flow reactor under microwave irradiation, as illustrated in Fig. 1(a). First, $ZrCl_4$ (4 g) was dissolved in DMF (108 mL), and then acetic acid (40 mL, the modulator) and water (10 mL) were added under stirring. Separately, 1,4-benzenedicarboxylic acid (4 g) was dissolved in 80 mL of DMF. The prepared two solutions were then delivered to the microwave reactor (M1-L213B, Midea, China) using two microfluidic syringe pumps. The flow rates of the two pumps were set at 1180 and 980 μL·min^{-1}, respectively, to ensure the 10 min residence time of the reaction mixture under microwave irradiation. The microwave reactor was operated at 350 W (2.45 GHz), and the reaction temperature was maintained at 120 °C. After the synthesis, the resulting product was separated by centrifugation and washed twice using DMF at 60 °C and twice using ethanol at 50 °C, then vacuum-dried at 150 °C for 24 h to give the pristine UIO-66 MOF.

2.3 PSM of UIO-66 by secondary construction

A previous PSM method was modified [24,25] to graft benzenesulfonic acid ($PhSO_3H$) on the pristine UIO-66, as illustrated in Figs. 1(b)–1(d). In detail, dry UIO-66 (1 g) was dispersed in dichloromethane (60 mL) under stirring at 5 °C. Subsequently, 4-chlorobenzenesulfonic acid in dichloromethane was added dropwise to the

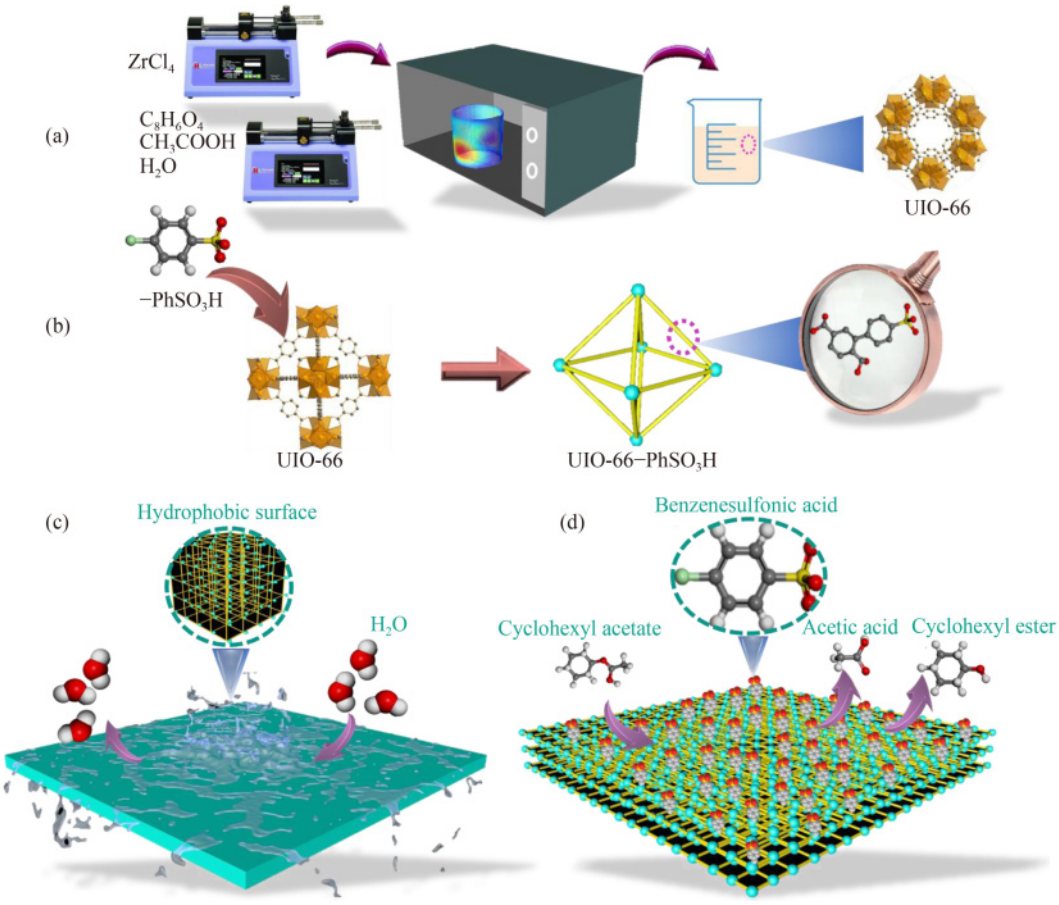

Fig. 1 Schematic diagram of (a) preparation for UIO-66, (b) preparation for UIO-66−$PhSO_3H$, (c) a hydrophobic surface, and (d) the hydrolysis reaction.

dispersion of UIO-66. The loading amount of 4-chlorobenzenesulfonic acid was varied to change the loading amount of $PhSO_3H$ on UIO-66, i.e., 1–5 wt %. After the synthesis, the mixture was filtered and washed with water, acetone, and ethanol, then vacuum-dried at 200 °C for 24 h, and the resulting material was denoted as UIO-66−$PhSO_3H$. Relevant synthesis parameters including of the mass ratio of 4-chlorobenzenesulfonic acid to UIO-66 (1–5 wt %), reaction temperature (−5–15 °C) and reaction time (15–90 min) were varied to optimize the process. Similarly, a control catalyst was prepared using chlorosulfonic acid to graft sulfonic acid groups (–SO_3H) on UIO-66 MOF, i.e., UIO-66−SO_3H, which was prepared using the same method above by replacing $PhSO_3H$ with sulfonic acid.

2.4 Characterization of materials

The structure of the materials under investigation was characterized by Fourier transform infrared spectroscopy (FTIR, Thermo Scientific Nicolet iS20, USA). Scanning was performed in the range of 400–4000 cm^{-1} using the potassium bromide (KBr) tablet method. The crystalline structure of the materials was determined by X-ray diffraction (XRD, Miniflex-600, Japan) analysis in the range of 3°–60°. The chemical composition of the sulfonated MOFs was analyzed by X-ray emission spectrometer (XPS, Thermo Scientific K-Alpha, USA). The S content of the sulfonated MOFs was measured and analyzed using an elemental analyzer (Elementar Vario EL CUBE, Elementar, Germany). The morphology and lattice characteristics of the MOF crystals were analyzed by scanning electron microscopy (SEM) and transmission electron microscopy (TEM). The thermogravimetric analysis (TGA) of the samples was performed using a thermogravimetric analyzer (NETZSCH STA 449 F5, Germany) under N_2 (at 5 $mL \cdot min^{-1}$) with a heating rate at 5 $°C \cdot min^{-1}$. Textural properties of the materials were analyzed using N_2 physisorption analysis (Micromeritics ASAP 2460, USA). Relevant porous properties were determined by the Brunauer–Emmett–Teller (BET) method and the Horvath–Kawazoe method.

2.5 Catalysis

In catalytic hydrolysis of cyclohexyl acetate to cyclohexanol, water and cyclohexyl acetate (cyclohexyl acetate to water ratios = 3 wt %) were charged into a high-pressure batch reactor (TCGF-50, Yuhua, China), then the catalyst (5 wt %) was added. The reactor was

pressurized using of N_2 (at 20 bar), and the reaction was performed at 100 °C. After the reaction, the reactor was cooled to room temperature, and acetone (20 mL) was added to the reaction mixture to increase the solubility of cyclohexanol in the aqueous phase. The catalyst was then removed by centrifugation, and the reaction mixture analyzed by gas chromatography (Trace 1300, Thermo Scientific, USA) with the flame ionization detector and wax capillary column (30.0 m × 250 μm × 0.25 μm). In the reusability tests, the recycled catalyst (which is separated by centrifugation) was washed twice using acetone and ethanol, and dried under vacuum at 200 °C for 24 h, then used again in the catalysis under the same condition. The conversion of cyclohexyl acetate and selectivity to cyclohexanol were calculated according to Eqs. S(1) and S(2) (cf. ESM).

3 Results and discussion

3.1 Characterization

Characterization of materials is shown in Fig. 2. Figure 2(a) shows the IR spectra of samples under investigation. In detail, the band at wavenumber of about 1700 cm^{-1} corresponds to the stretching vibration of C=O. The IR bands at 743, 667 and 550 cm^{-1} are attributed to presence of Zr–O–C coordination [7]. The vibration peaks at 1391 and 1581 cm^{-1} can be observed, corresponding to the symmetric stretching vibration and asymmetric stretching vibration of O–C–O, respectively [26]. The vibration peaks of the C–C bond of the benzene ring appeared at 1506 cm^{-1}. Due to the increase in the number of benzene rings in UIO-66−$PhSO_3H$ (3 wt %) after the secondary construction, the vibration peak at 1506 cm^{-1} is slightly stronger than that of UIO-66. In addition, compared to the IR spectrum of UIO-66, that of UIO-66−$PhSO_3H$ (3 wt %) shows additional peaks at 1134, 1127, and 1270 cm^{-1}, which are attributed to the stretching of S–O bond and O=S=O symmetric and asymmetric stretching vibrations, respectively [27]. FTIR characterization results suggest that benzenesulfonic acid was grafted successfully on the organic linker of UIO-66. In addition, the wide IR bands of –OH appeared at ca. 3100 cm^{-1}, which was due to the existence of water molecules in the samples. Comparatively, the band of UIO-66−$PhSO_3H$ (3 wt %) was less significant in comparison with that of the pristine UIO-66 and UIO-66−SO_3H (3 wt %), suggesting that UIO-66−$PhSO_3H$ (3 wt %) is rather hydrophobic. XRD analysis of the three samples showed that they all have similar crystalline properties, being similar to that reported in the literature (Fig. 2(b)) [28,29]. The two strong diffraction peaks at $2\theta = 7.4°$ and 8.3°, respectively, are the characteristic diffraction peaks of the (111) and (200) crystal planes of UIO-66 [30]. In comparison with UIO-66, changes in the XRD diffraction patterns of UIO-66−$PhSO_3H$ (3 wt %) and UIO-66−SO_3H (3 wt %) were not significant, indicating that the crystal structure of UIO-66 was well preserved after the PSM secondary construction.

XPS analysis was performed as well to know the surface chemical compositions of the three materials, as

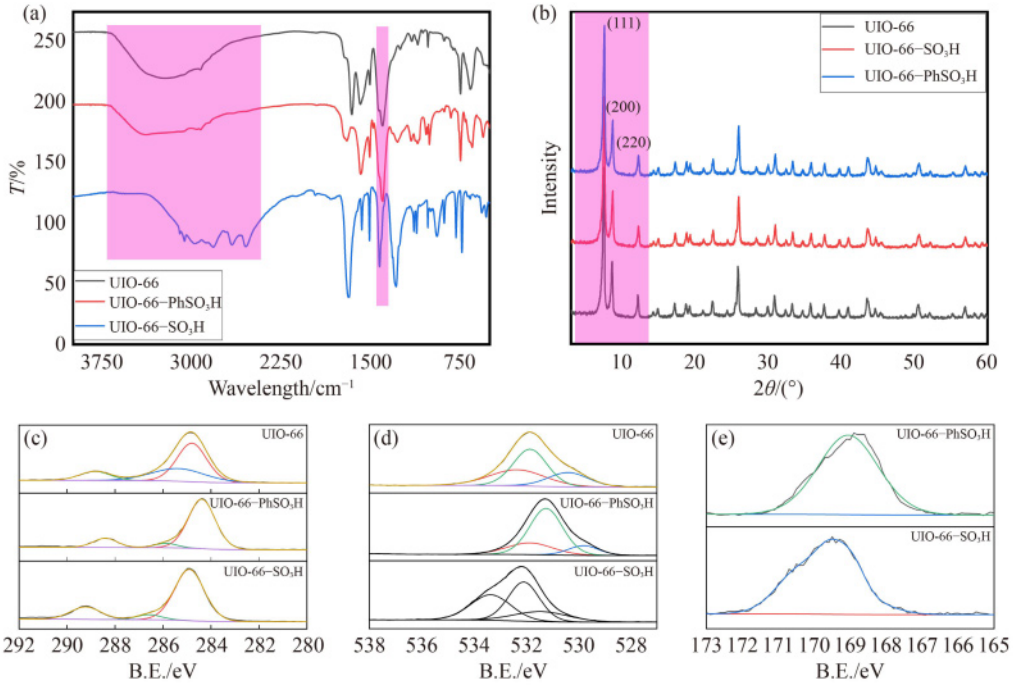

Fig. 2 Structure analysis of UIO-66, UIO-66−SO_3H (3 wt %), and UIO-66−$PhSO_3H$ (3 wt %) by (a) FTIR, (b) XRD, and XPS spectra of (c) C 1s, (d) O 1s, and (e) S 2p.

shown in Figs. 2(c)–2(e) (the scan survey is shown in Fig. S1, cf. ESM). Figure 2(c) shows the C 1s spectrum of the pristine UIO-66, which can be fitted using three peaks, corresponding to C=O (288.68 eV), C–O (285.48 eV), C–C (284.78 eV), respectively [31,32]. Compared to UIO-66, the position of each characteristic peak in the C 1s spectra of UIO-66−$PhSO_3$ (3 wt %) and UIO-66−SO_3H (3 wt %) showed the redshift, which may be due to the introduction of the grafted functional groups. Figure 2(d) shows the O 1s spectra of the three materials, presenting three characteristic peaks of C–OH, C=O, and C–O–C. S content was detected by XPS (Fig. 2(e)), showing the S $2p_{3/2}$ peak position at the binding energy of around 168.11 eV, which suggests the presence of surface –SO_3H group [33]. The textual properties of UIO-66, UIO-66−SO_3H (3 wt %), and UIO-66−$PhSO_3H$ (3 wt %) were measured using N_2 physisorption. The isotherms of the three materials are shown in Fig. S2 (cf. ESM), presenting the type IV isotherms for microporous materials. Compared to the BET specific surface area of UIO-66, after the surface modification using –SO_3H group, the specific surface area of UIO-66−SO_3H (1051 $cm^2 \cdot g^{-1}$) did not change, as well as the specific pore volume, as shown in Table 1. Conversely, the specific surface area of UIO-66−$PhSO_3H$ MOFs decreased gradually (from 1050 to 730 $cm^2 \cdot g^{-1}$) with an increase of benzenesulfonic acid loading (from 1 wt % to 4 wt %) because that the grafted benzenesulfonic acid group on the linkers could occupy pore space in the framework [24]. All the relevant characterization data show the evidence of successful introduction of surface groups to UIO-66 using the developed PSM method.

Figure 3 shows the TGA profiles of UIO-66, UIO-66−SO_3H (3 wt %), and UIO-66−$PhSO_3H$ (3 wt %). As shown in Fig. 3(a), two distinct weight loss steps can be observed for UIO-66 between 20 and 800 °C. The weight loss between 20 and 100 °C can attributed to the desorption of solvent molecules from the framework and structural defects, that is, water and ethanol [22]. The weight loss of UIO-66 was very steep at 100–200 °C, which was due to the severe dehydroxylation of the zirconium-oxygen clusters in the framework [34,35]. The final weight loss of UIO-66 at 200–500 °C can be due to the framework collapse. The TGA curve of UIO-66−SO_3H (3 wt %) is shown in Fig. 3(b), in which the initial weigh loss at low temperatures was not found. The sharp drop around 300 °C can be attributed to the sudden damage of its framework, suggesting that the modification using sulfonic acid made the framework less stable. Comparatively, the weight loss of UIO-66−$PhSO_3H$ (3 wt %) was relatively insignificant at 200–500 °C, as shown in Fig. 3(c), confirming its stability. The final weight loss at around 500 °C was comparable to that of the pristine UIO-66, which is attributed to the complete destruction of its framework [36]. The findings from TGA show that after the secondary construction of UIO-66, UIO-66−$PhSO_3H$ (3 wt %) prepared by benzenesulfonic acid modification was combatively the most stable material, making it suitable for catalytic applications.

SEM and TEM analyses of UIO-66, UIO-66−$PhSO_3H$ (3 wt %) and UIO-66−SO_3H (3 wt %) were performed to study their macroscopic and microscopic morphologies (Fig. 4). SEM micrographs of the three materials are shown in Figs. 4(a-I), 4(b-I) and 4(c-I), and one can see that the individual crystals all have similar spherical morphologies with particle sizes of about 100 nm. The

Table 1 Textural properties of the materials under investigation

Samples	S_{BET}/($cm^2 \cdot g^{-1}$)	D_{meso}/nm	V/($cm^3 \cdot g^{-1}$)
UIO-66	1051	2.1	0.5
UIO-66−SO_3H (3 wt %)	1051	2.1	0.5
UIO-66−$PhSO_3H$ (1 wt %)	1050	2.0	0.5
UIO-66−$PhSO_3H$ (2 wt %)	1038	2.1	0.5
UIO-66−$PhSO_3H$ (3 wt %)	648	2.4	0.4
UIO-66−$PhSO_3H$ (4 wt %)	730	2.3	0.4

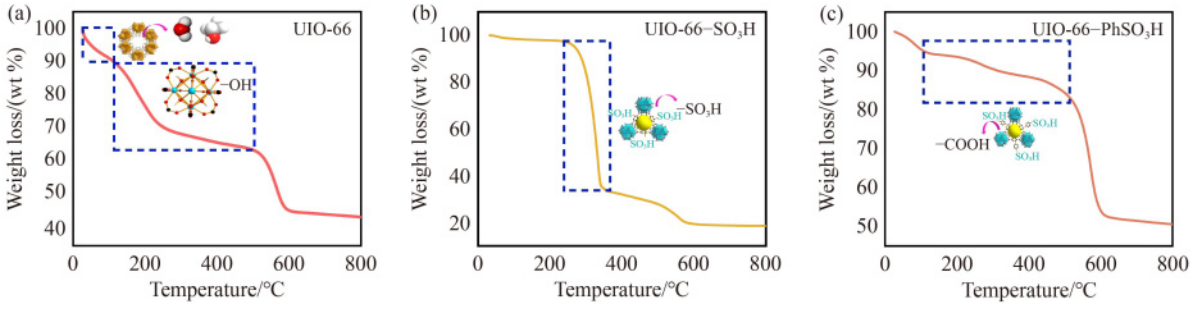

Fig. 3 TGA profiles of (a) UIO-66, (b) UIO-66−SO_3H (3 wt %), and (c) UIO-66−$PhSO_3H$ (3 wt %).

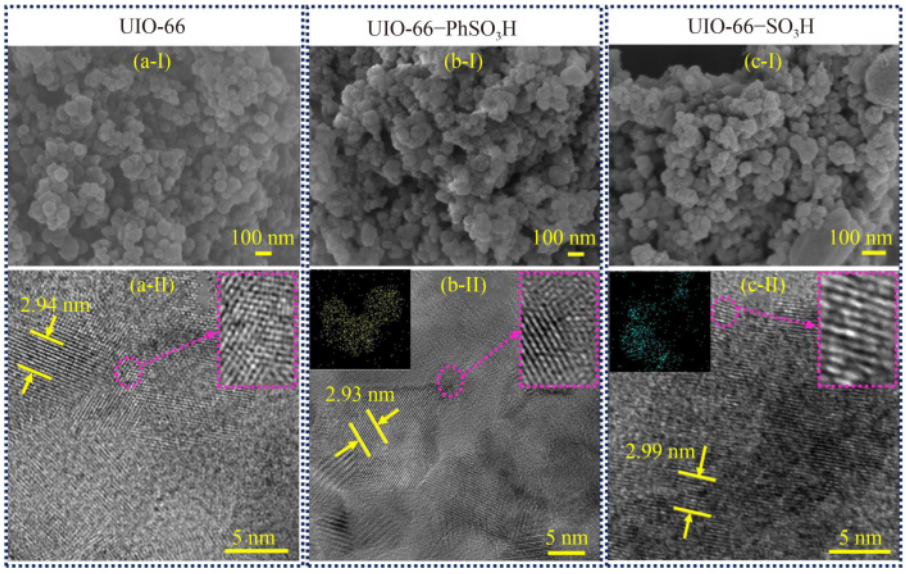

Fig. 4 Topography (I: SEM; II: TEM) of (a) UIO-66, (b) UIO-66−$PhSO_3H$ (3 wt %), and (c) UIO-66−SO_3H (3 wt %) (insets: relevant lattice fringes and EDS mapping analysis for S content in UIO-66−SO_3H and UIO-66−$PhSO_3H$).

crystal sizes of UIO-66 prepared by the microwave method are larger than that reported in the literature (about 90 nm) [22,23]. This is due to the competition between the organic ligands and acetic acid (modulator) at Zr nodes, which is prone to encourage the growth of large crystals [37]. The particle sizes of the three samples were measured by dynamic light scattering (DLS) as well, as shown in Fig. S3 (cf. ESM). The DLS measured particle size distribution of UIO-66 suggests that it has the average particle size of about 495 nm (Fig. S3(a)), which is significantly larger than that by SEM due to the crystal aggregation. Comparatively, the DLS particle sizes of UIO-66−$PhSO_3H$ (about 255 nm) (Fig. S3(b)) and UIO-66−SO_3H (about 396 nm) (Fig. S3(c)) are smaller than that of the pristine UIO-66. This is reasonable since UIO-66−$PhSO_3H$ (3 wt %) and UIO-66−SO_3H (3 wt %) are produced by PSM of the pristine UIO-66, and during the treatments aggregated UIO-66 crystals could be separated. TEM analysis of the three samples (Figs. 4(a-II), 4(b-II) and 4(c-II)) shows that they are well crystalized, as evidenced by the clear lattice fringes with a lattice spacing of 0.295 nm, corresponding to a stack of the (101) planes of the tetragonal ZrO_2 [38]. Energy dispersive spectroscopy (EDS) mapping analysis was conducted for UIO-66−$PhSO_3H$ and UIO-66−SO_3H (insets in Figs. 4(b-II) and 4(c-II)), showing that the sulfur (S) element is uniformly distributed on the surface of UIO-66−$PhSO_3H$ (3 wt %) and UIO-66−SO_3H (3 wt %), which proves that the sulfonic acid group was successfully introduced into the structure of UIO-66 through the PSM secondary construction method.

The ratio of 4-chlorobenzenesulfonic acid to UIO-66, synthesis temperature and time were varied to investigate their effects on grafting $PhSO_3H$ on the surface of UIO-66, which is characterized by the S content of the resulting materials, as shown in Fig. S4 (cf. ESM). The results show that in the synthesis at 0 °C (for 1 h) an increase in the 4-chlorobenzenesulfonic acid to UIO-66 mass ratio was initially beneficial to increase the S content in the resulting materials. When the ratio reached 3, the S content of UIO-66−$PhSO_3H$ reaches saturation with the highest loading of 4.68 wt %, and further increase in the ratio to 5 did not increase the S content. This can be due to the steric hindrance effect by the grafted benzenesulfonic acid group, i.e., upon saturation then the available UIO-66 surface is used up, and hence the benzenesulfonic acid in the system could not be grafted in UIO-66 anymore. Regarding the effect of the synthesis temperature, the findings show that 5 °C was the optimum temperature for grafting the surface group on UIO-66 (under the condition of the 4-chlorobenzenesulfonic acid to UIO-66 mass ratio = 3 wt % and synthesis time = 1 h), which resulted in the loading of $PhSO_3H$ of about 4.67 wt % (Fig. S4(b)). At low temperatures of <5 °C, the molecular motion is slow and the reaction between benzenesulfonic acid and the linkers of UIO-66 is slow, resulting in ineffective loading of the $PhSO_3H$ group. Conversely, at the high temperatures of >5 °C, the grafting process was affected adversely by the exothermicity of the reaction [39]. Under the condition of the 4-chlorobenzenesulfonic acid to UIO-66 mass ratio = 3 wt % and synthesis temperature = 0 °C), it was found that synthesis time of 60 min was appropriate for the loading of the $PhSO_3H$ group on UIO-66 (Fig. S4(c)), suggesting that sufficient synthesis time was required for the saturation of UIO-66 surface by the benzenesulfonic acid. Finally, based on the maximum loading of the S content on the surface of UIO-66 at about 4.9 wt %, the optimum synthesis condition for making UIO-66−$PHSO_3H$ was identified as: the 4-chlorobenzenesulfonic

acid to UIO-66 mass ratio = 3 wt %, synthesis temperature = 5 °C and synthesis time = 1 h. For UIO-66−$PHSO_3H$ with a S content of 4.9 wt %, its water contact angle was measured to be 98°. Conversely, the contact angles of UIO-66 and UIO-66−SO_3H are smaller than 90°, i.e., 67° and 74°, respectively, as shown in the insets of Fig. S3. The findings show that the introduction of benzenesulfonic acid to the surface of UIO-66 can make the material hydrophobic.

3.2 Catalytic hydrolysis of cyclohexyl acetate over the developed catalysts

The catalytic activity of the developed UIO-66−$PhSO_3H$ catalysts with different S contents was investigated using catalytic hydrolysis of cyclohexyl acetate to cyclohexanol (Fig. 5). The findings show that an increase in the loading of the surface $PhSO_3H$ on UIO-66 from 1 to 4 wt % caused an increase in the conversion of cyclohexyl acetate from 66% to 85.6% (Fig. 5(a)). However, when the $PhSO_3H$ loading was increased to 5 wt %, the conversion of cyclohexyl acetate decreased to 65.7%. This could be attributed to the steric hindrance caused by the concentrated benzenesulfonic acid group on the catalyst surface, making the accessibility of the active sites of UIO-66−$PhSO_3H$ reduced to water molecules. In the catalytic system, water as one of the reactants needs to be in sufficient contact with the substrate intermediate (Fig. 5(b)). Water molecules provide sufficient hydroxyl groups to convert the intermediate to cyclohexanol. Hence, high concentration of benzenesulfonic acid leads to strong hydrophobicity, which repels water molecules, resulting in the reduction of the cyclohexyl acetate conversion. Conversely, the selectivity to cyclohexanol of the UIO-66−$PhSO_3H$ catalysts under investigation was rather comparable at about 99%. The results above suggest that the catalytic activity of UIO-66−$PhSO_3H$ regarding conversion is affected by the concentration of the surface groups.

To test the hydrothermal stability of the UIO-66−$PhSO_3H$ (3 wt %) catalyst, cyclic catalytic tests were performed using different catalysts with a high water to cyclohexyl acetate mass ratio of 3. As shown in Fig. 6, the pristine UIO-66 was able to promote the catalysis. It is due to a presence of structure defectives, which is weakly acidic and was produced due to the use of acetic acid as the modulator during the synthesis of UIO-66. Regarding the UIO-66−SO_3H (3 wt %) catalyst, the conversion of cyclohexyl acetate over it decreased by about 11% after three repetitive uses, that is, the conversion dropped from 72.7% for the first cycle to 64.8% for the third cycle. For UIO-66−$PhSO_3H$ (3 wt %), after three tests, insignificant decreases in the conversion rate of about 1.2% (from 85.4% to 84.3%) and selectivity of about 1.5% (from 98.5% to 97%) were measured, proving that the developed UIO-66−$PhSO_3H$ catalyst was rather stable in the aqueous catalytic system. During the hydrolysis of cyclohexyl acetate, an increase in the amount of water used in the system is beneficial to the catalysis, as shown in Fig. S5 (cf. ESM), by increasing the water to cyclohexyl acetate mass ratio from 1:3 to 2:1, the conversion of cyclohexyl acetate also increased from 55.4% to 69%. Surface modification of UIO-66 using the -$PhSO_3H$ group cannot only introduce the Brønsted acidity to the MOF for promoting hydrolysis catalysis effectively, but also make the MOF hydrophobic to maintain its structural stability in the presence of a large amount of water. In addition, the hydrophobic nature of UIO-66−$PhSO_3H$ can also increase its affinity to the oily molecule cyclohexyl acetate, which benefits the reaction. However, since water was the key reactant of the catalytic system as well, hence there is a trade-off between activity and stability. As discussed above, when excessive surface $PhSO_3H$ loading was used, the superhydrophobic structure of the UIO-66−$PhSO_3H$ catalyst can reject water, which does not favor the catalytic hydrolysis. Therefore, appropriate modification of UIO-66 using the benzenesulfonic acid group is needed to tune its hydrophobicity to balance the structural stability and catalytic activity.

Based on the results from the catalytic tests, the relationship between the stability and activity was analyzed in detail, as shown in Fig. 7. For UIO-66−SO_3H,

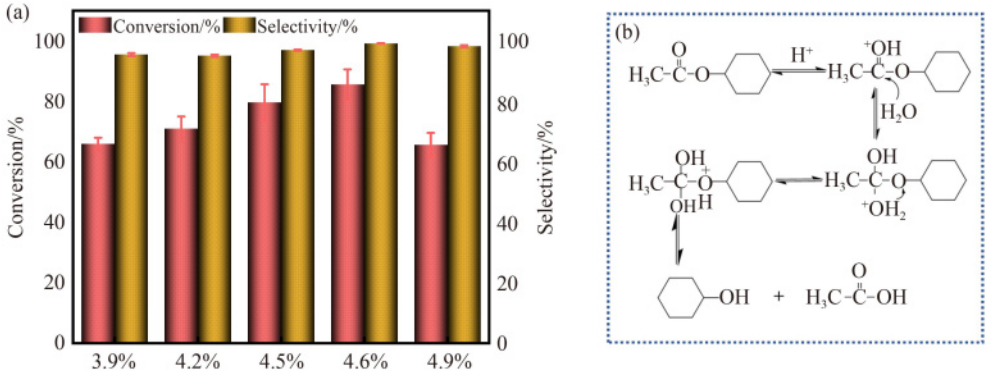

Fig. 5 (a) Conversion and selectivity of the hydrolysis of cyclohexyl acetate to cyclohexanol over the UIO-66−$PhSO_3H$ catalysts with different $PhSO_3H$ loading, and (b) the catalytic mechanism.

the surface modification of UIO-66 using the sulfonic acid group imparts Brønsted acidity to MOFs, as well as making it hydrophilic (with the measured contact angle = 74°, Fig. 7(a)). In an aqueous system, the hydrophilic catalyst can attract water to coordinate with its structural defects, which is not beneficial to maintain its structural integrity and catalytic activity. In addition, during the hydrolysis of cyclohexyl acetate acetic acid can be produced which can, together with water, coordinate with the framework defects of UIO-66−SO_3H. Loss of the structural defects due to coordination can lead to the reduced catalytic performance. Also, during the catalyst regeneration process (at 200 °C under vacuum for 24 h) the coordinated water and acetic acid are removed which can destroy the framework partially (Fig. 7(b)). After the repetitive regeneration during the cyclic stability tests, the continuous erosion of the framework structure can be detrimental to the long-term stability of the UIO-66−SO_3H catalyst. Post reaction characterization of the materials shows that after the stability tests UIO-66−SO_3H lost its crystallinity and specific surface area significantly. Compared to UIO-66 and UIO-66−$PhSO_3H$ (3 wt %), the XRD diffraction pattern of UIO-66−SO_3H shows the presence of amorphous phase (Fig. S6(a), cf. ESM), and its BET surface areas dropped to 678 $cm^2 \cdot g^{-1}$, being considerably lower than its original value of 1051 $cm^2 \cdot g^{-1}$.

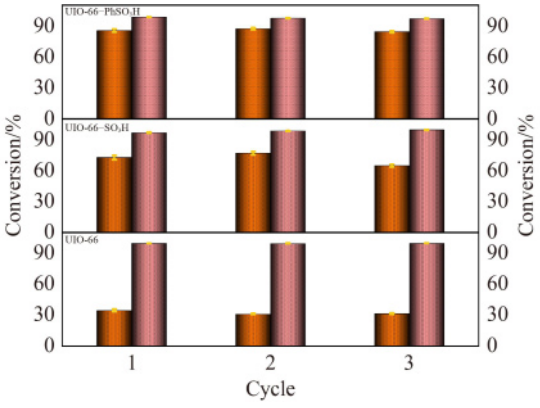

Fig. 6 Reusability of the UIO-66, UIO-66−SO_3H (3 wt %), UIO-66−$PhSO_3H$ (3 wt %) catalysts.

Comparatively, the UIO-66−$PhSO_3H$ (3 wt %) catalyst is hydrophobic with the contact angle of 98°, and hence the hydrophobic surface groups of UIO-66−$PhSO_3H$ (3 wt %) can prevent the attack of water molecules and maintain the stability of its structure effectively. Figure S6(b) and Table S1 show that the relevant physiochemical properties of the used UIO-66−$PhSO_3H$ (3 wt %) were comparable to that of the fresh one. In detail, the specific BET surface area of UIO-66−$PhSO_3H$ (3 wt %) was not reduced after the stability test, and the XRD pattern of the used UIO-66−$PhSO_3H$ (3 wt %) was also comparable to that of the fresh one. The morphology of the used UIO-66−$PhSO_3H$ (3 wt %) catalyst was analyzed by TEM as well (Fig. S6(c)), showing the intact morphology after the stability test. Specially, the lattice fringes of the used UIO-66−$PhSO_3H$ (3 wt %) catalyst can be observed clearly (Fig. S6(d)), confirming the preserved crystallinity of the used UIO-66−$PhSO_3H$ (3 wt %). In addition, the surface S element of the used was analyzed by EDS (Fig. S6(e)), showing uniformly distributed S content on the surface of the used catalyst.

4 Conclusions

We report a facile PSM strategy for making stable

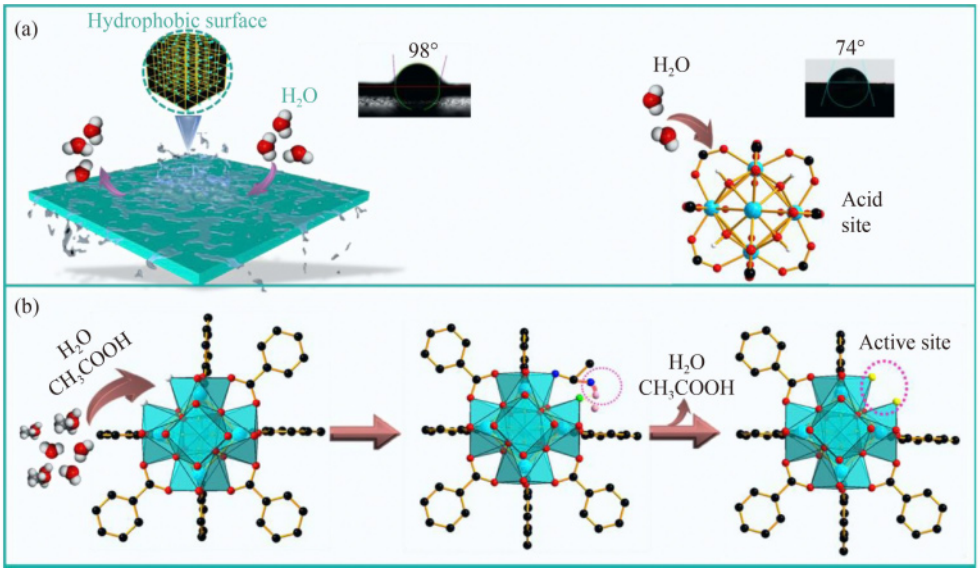

Fig. 7 Schematic diagram for the stability mechanism of the catalysts: (a) the contact angle of catalysts and the mechanism of action between water molecules and catalysts, and (b) catalyst regeneration mechanism.

UIO-66 catalyst with Brønsted acidity for catalysis in aqueous phase. The PSM secondary construction method was used to functionalize the UIO-66 MOF using benzenesulfonic acid to give the UIO-66−$PhSO_3H$ catalyst. Due to the presence of benzenesulfonic acid groups in UIO-66−$PhSO_3H$ it is hydrophobic with a large contact angle of 98°, making it stable in applications involving water. UIO-66−$PhSO_3H$ was tested using a model reaction of hydrolysis of cyclohexyl acetate (to cyclohexanol), after three consecutive tests, only insignificant decreases in the conversion rate (i.e., by about 1.3%, from 85.4% to 84.3%) and selectivity of about 1.5% (i.e., by about 1.5%, from 98.5% to 97%) were measured. The findings suggest that the introduction of benzenesulfonic acid groups could effectively avoid the attack of water molecules to the catalyst based on UIO-66 MOF, sustaining the stability of UIO-66−$PhSO_3H$ during the reaction, which was evidenced by the comparative characterization of the fresh and used catalysts from the cyclic stability tests. This work demonstrated a practical and simple strategy to make stable Brønsted acid MOFs catalysts for further exploration in catalytic processes.

Acknowledgements This project has received funding from the European Union's Horizon 2020 Research and Innovation Program (Grant No. 872102). The Chinese colleagues thank the National Key R&D Program of China (Grant No. 2019YFE0123200). Fan X and Pan Q thank the International Science & Technology Cooperation Program of Hainan Province (Grant No. GHYF2022006) for the collaborative research.

Electronic Supplementary Material Supplementary material is available in the online version of this article at https://dx.doi.org/10.1007/s11705-022-2285-5 and is accessible for authorized users.

References

1. Cirujano F G, Llabres I X F X. Tuning the catalytic properties of UiO-66 metal–organic frameworks: from Lewis to defect-induced Bronsted acidity. Journal of Physical Chemistry Letters, 2020, 11(12): 4879–4890
2. Longa J R, Yaghi O M. The pervasive chemistry of metal–organic frameworks. Chemical Society Reviews, 2009, 38(5): 1213–1214
3. Wang C, An B, Lin W. Metal–organic frameworks in solid–gas phase catalysis. ACS Catalysis, 2019, 9(1): 130–146
4. Liu J, Chen L, Cui H, Zhang J, Zhang L, Su C Y. Applications of metal–organic frameworks in heterogeneous supramolecular catalysis. Chemical Society Reviews, 2014, 43(16): 6011–6061
5. Dhakshinamoorthy A, Santiago-Portillo A, Asiri A M, Garcia H. Engineering UiO-66 metal organic framework for heterogeneous catalysis. ChemCatChem, 2019, 11(3): 899–923
6. Jiao L, Wang Y, Jiang H L, Xu Q. Metal–organic frameworks as platforms for catalytic applications. Advanced Materials, 2018, 30(37): e1703663
7. Wang Y, Li L, Dai P, Yan L, Cao L, Gu X, Zhao X. Missing-node directed synthesis of hierarchical pores on a zirconium metal–organic framework with tunable porosity and enhanced surface acidity via a microdroplet flow reaction. Journal of Materials Chemistry A: Materials for Energy and Sustainability, 2017, 5(42): 22372–22379
8. Jiang J, Yaghi O M. Bronsted acidity in metal–organic frameworks. Chemical Reviews, 2015, 115(14): 6966–6997
9. Corma A. Inorganic solid acids and their use in acid-catalyzed hydrocarbon reactions. Chemical Reviews, 1995, 95(3): 559–614
10. Furukawa H, Muller U, Yaghi O M. "Heterogeneity within order" in metal–organic frameworks. Angewandte Chemie International Edition, 2015, 54(11): 3417–3430
11. Shepherd N D, Wang T, Ding B, Beves J E, D'Alessandro D M. Visible light stimulated bistable photo-switching in defect engineered metal–organic frameworks. Inorganic Chemistry, 2021, 60(16): 11706–11710
12. Tanabe K K, Cohen S M. Postsynthetic modification of metal–organic frameworks—a progress report. Chemical Society Reviews, 2011, 40(2): 498–519
13. Deng H, Doonan C J, Furukawa H, Ferreira R B, Towne J, Knobler C B, Wang B, Yaghi O M. Multiple functional groups of varying ratios in metal–organic frameworks. Science, 2010, 327(5967): 846–850
14. Zhang Y B, Furukawa H, Ko N, Nie W, Park H J, Okajima S, Cordova K E, Deng H, Kim J, Yaghi O M. Introduction of functionality, selection of topology, and enhancement of gas adsorption in multivariate metal–organic framework-177. Journal of the American Chemical Society, 2015, 137(7): 2641–2650
15. Chen J, Li K, Chen L, Liu R, Huang X, Ye D. Conversion of fructose into 5-hydroxymethylfurfural catalyzed by recyclable sulfonic acid-functionalized metal–organic frameworks. Green Chemistry, 2014, 16(5): 2490–2499
16. Desidery L, Yusubov M S, Zhuiykov S, Verpoort F. Fully-sulfonated hydrated UiO66 as efficient catalyst for ethyl levulinate production by esterification. Catalysis Communications, 2018, 117: 33–37
17. Morales G, Athens G, Chmelka B, Vangrieken R, Melero J. Aqueous-sensitive reaction sites in sulfonic acid-functionalized mesoporous silicas. Journal of Catalysis, 2008, 254(2): 205–217
18. da Silva Rocha K A, Hoehne J L, Gusevskaya E V. Phosphotungstic acid as a versatile catalyst for the synthesis of fragrance compounds by alpha-pinene oxide isomerization: solvent-induced chemoselectivity. Chemistry, 2008, 14(20): 6166–6172
19. Liu L, Tao Z P, Chi H R, Wang B, Wang S M, Han Z B. The applications and prospects of hydrophobic metal–organic

frameworks in catalysis. Dalton Transactions, 2021, 50(1): 39–58
20. Cai M, Li Y, Liu Q, Xue Z, Wang H, Fan Y, Zhu K, Ke Z, Su C Y, Li G. One-step construction of hydrophobic MOFs@COFs core-shell composites for heterogeneous selective catalysis. Advanced Science, 2019, 6(8): 1802365
21. Isaka Y, Kawase Y, Kuwahara Y, Mori K, Yamashita H. Two-phase system utilizing hydrophobic metal–organic frameworks (MOFs) for photocatalytic synthesis of hydrogen peroxide. Angewandte Chemie International Edition, 2019, 58(16): 5402–5406
22. Vo K, Le V N, Yoo K S, Song M, Kim D, Kim J. Facile Synthesis of UiO-66(Zr) using a microwave-assisted continuous tubular reactor and its application for toluene adsorption. Crystal Growth & Design, 2019, 19(9): 4949–4956
23. Taddei M, Steitz D A, Bokhoven J A, Ranocchiari M. Continuous-flow microwave synthesis of metal–organic frameworks: a highly efficient method for large-scale production. Chemistry, 2016, 22(10): 3245–3249
24. Li H, Deng Q, Chen H, Cao X, Zheng J, Zhong Y, Zhang P, Wang J, Zeng Z, Deng S. Benzenesulfonic acid functionalized hydrophobic mesoporous biochar as an efficient catalyst for the production of biofuel. Applied Catalysis A: General, 2019, 580(25): 178–185
25. Li B, Zhang Y, Ma D, Li L, Li G, Li G, Shi Z, Feng S. A strategy toward constructing a bifunctionalized MOF catalyst: post-synthetic modification of MOFs on organic ligands and coordinatively unsaturated metal sites. Chemical Communications, 2012, 48(49): 6151–6153
26. Han Y, Liu M, Li K, Zuo Y, Wei Y, Xu S, Zhang G, Song C, Zhang Z, Guo X. Facile synthesis of morphology and size-controlled zirconium metal–organic framework UiO-66: the role of hydrofluoric acid in crystallization. CrystEngComm, 2015, 17(33): 6434–6440
27. Ordomsky V V, Sushkevich V L, Schouten J C, van der Schaaf J, Nijhuis T A. Glucose dehydration to 5-hydroxymethylfurfural over phosphate catalysts. Journal of Catalysis, 2013, 300: 37–46
28. Qiu J, Feng Y, Zhang X, Jia M, Yao J. Acid-promoted synthesis of UiO-66 for highly selective adsorption of anionic dyes: adsorption performance and mechanisms. Journal of Colloid and Interface Science, 2017, 499: 151–158
29. Morris W, Wang S, Cho D, Auyeung E, Li P, Farha O K, Mirkin C A. Role of modulators in controlling the colloidal stability and polydispersity of the UiO-66 metal–organic framework. ACS Applied Materials & Interfaces, 2017, 9(39): 33413–33418
30. Lin Foo M, Horike S, Fukushima T, Hijikata Y, Kubota Y, Takata M, Kitagawa S. Ligand-based solid solution approach to stabilisation of sulphonic acid groups in porous coordination polymer $Zr_6O_4(OH)_4(BDC)_6$ (UiO-66). Dalton Transactions, 2012, 41(45): 13791–13794
31. Smith J L, Herman R G, Terenna C R, Galler M R, Klier K. Sorption of nitrogen bases and XPS study of mesoporous solid acid SBA-15. Journal of Physical Chemistry A, 2004, 108(1): 39–46
32. Chellappan S, Aparna K, Chingakham C, Sajith V, Nair V. Microwave assisted biodiesel production using a novel Brønsted acid catalyst based on nanomagnetic biocomposite. Fuel, 2019, 246(15): 268–276
33. Jeremy L, Smith R G H, Terenna C R, Galler M R, Klier K. Sorption of nitrogen bases and XPS study of mesoporous solid acid SBA-15. The Journal of Chemical Physics A, 2004, 108(1): 39–46
34. Wißmann G, Schaate A, Lilienthal S, Bremer I, Schneider A M, Behrens P. Modulated synthesis of Zr-fumarate MOF. Microporous and Mesoporous Materials, 2012, 152: 64–70
35. Liu X, Zhao X, Zhou M, Cao Y, Wu H, Zhu J. Highly stable and active palladium nanoparticles supported on a mesoporous UiO66@reduced graphene oxide complex for practical catalytic applications. European Journal of Inorganic Chemistry, 2016, 2016(20): 3338–3343
36. Chavan S M, Shearer G C, Svelle S, Olsbye U, Bonino F, Ethiraj J, Lillerud K P, Bordiga S. Synthesis and characterization of amine-functionalized mixed-ligand metal–organic frameworks of UiO-66 topology. Inorganic Chemistry, 2014, 53(18): 9509–9515
37. Vakili R, Xu S, Al-Janabi N, Gorgojo P, Holmes S M, Fan X. Microwave-assisted synthesis of zirconium-based metal organic frameworks (MOFs): optimization and gas adsorption. Microporous and Mesoporous Materials, 2018, 260: 45–53
38. Ambrosi M, Fratini E, Canton P, Dankesreiter S, Baglioni P. Bottom-up/top-down synthesis of stable zirconium hydroxide nanophases. Journal of Materials Chemistry, 2012, 22(44): 23497–23505
39. Russo V, Milicia A, Di Serio M, Tesser R. Falling film reactor modelling for sulfonation reactions. Chemical Engineering Journal, 2019, 377: 120464